Effects of Trade-Wind Strength and Direction on the Leeside Circulations and Rainfall of the Island of Hawaii

YANG YANG AND YI-LENG CHEN

Department of Meteorology, School of Ocean and Earth Science and Technology, University of Hawaii at Manoa, Honolulu, Hawaii

FRANCIS M. FUJIOKA

Forest Fire Laboratory, U.S. Department of Agriculture, Riverside, California

(Manuscript received 4 September 2007, in final form 17 February 2008)

ABSTRACT

The leeside circulations and weather of the island of Hawaii were studied from the fifth-generation Pennsylvania State University–NCAR Mesoscale Model (MM5) land surface model simulations for eight strong (~7.9 m s^{-1}) and eight weak (~5.2 m s^{-1}) trade-wind days and for five days with southeasterly trades (~7.1 m s^{-1}) during summer 2004. The objective is to investigate the effects of trade-wind strength and directions on the leeside circulations and rainfall and the modification of these effects by the land surface thermal forcing. For the small wake on the lee side of the Kohala Mountains (1700 m, lower than the trade-wind inversion at 2000 m) over northern Hawaii, the hydraulic jump is present with stronger downslope winds and warmer and drier conditions on the lee side and a weaker westerly reversed flow offshore when trades are stronger. In contrast, the westerly reversed flow along the large wake axis off the central Kona leeside coast (behind massive mountains with tops >4000 m) is 1–1.5 m s^{-1} stronger and 200–300 m deeper with higher moisture content when trades are stronger. Over the Kona slopes, the daytime thermally direct circulation cell is more significant when trades are stronger because of descending airflow aloft with less cloudiness. In the evening, the convergence between the westerly reversed flow offshore along the wake axis and the offshore/katabatic flow in the Kona coastal region is more significant with higher evening rainfall when trades are stronger. During the day, the lee side of the Kohala Mountains is characterized by a reversed flow (~4 m s^{-1}) merging with sea-breeze circulations along the coast. When trades are stronger, the convergence between the anabatic winds and the descending flow from the upper slopes is greater. However, the simulated cloud water there is less under strong trades because of warmer and drier conditions due to significant adiabatic descent in the lee. At night, when trades are stronger, the combined downslope/katabatic flow prevails without a reversed flow offshore. Under a southeasterly trade-wind flow with a lower trade-wind inversion (1.5 km), the westerly reversed flow is shallower; the adiabatic descent aloft on the southwestern leeside areas is more significant with warmer temperatures (0.5 K), a larger negative potential vorticity maximum [0.2 potential vorticity units (PVU), 1 PVU = 10^{-6} K m^2 s^{-1} kg^{-1}], and a more pronounced anticyclonic vortex offshore. The westerly reversed flow off the Kona coast shifts northward.

1. Introduction

The island of Hawaii is the largest of the Hawaiian island chain, with a diameter of roughly 140 km. Its topography is dominated by two volcanic mountains, Mauna Loa and Mauna Kea (Fig. 1a), both exceeding 4100 m in elevation. Climatologically, east-northeasterly trade winds of 4–10 m s^{-1} are persistent (70%) throughout the year, especially in summer, with the maximum occurrence of 92% in August (Schroeder 1993).

For a stratified airflow past circular mountains without considering diabatic heating and surface friction, the Froude number (Fr = U/Nh, where U is the upstream wind speed, N is the Brunt–Väisälä frequency, and h is the height of the barrier) or nondimensional mountain height (1/Fr) is the control parameter for

Corresponding author address: Prof. Yi-Leng Chen, Department of Meteorology, University of Hawaii at Manoa, Honolulu, HI 96822.
E-mail: yileng@hawaii.edu

DOI: 10.1175/2008MWR2365.1

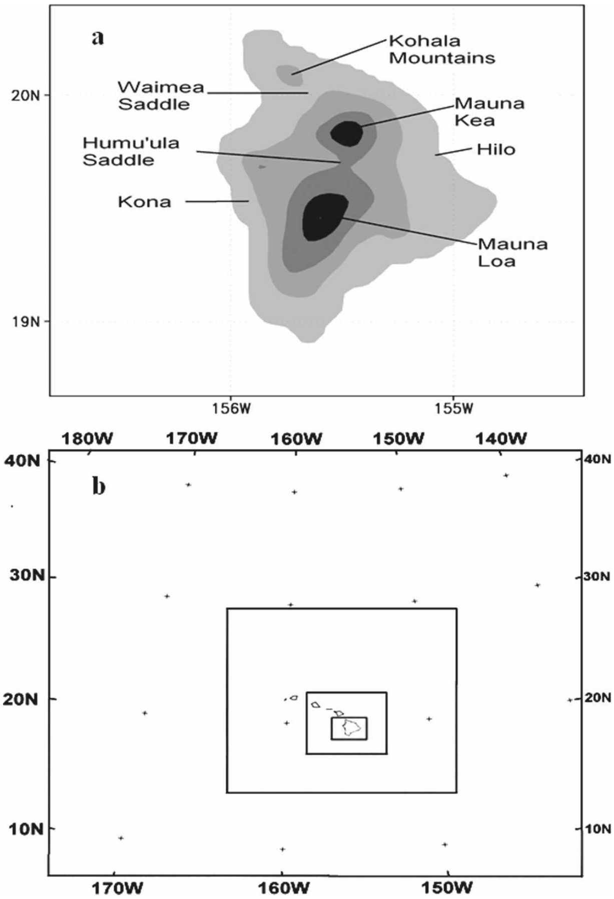

FIG. 1. (a) Island of Hawaii with terrain height shown by gray shading scale of 1000 m from light to dark (the same hereinafter). (b) The four nested domains with resolutions of 81, 27, 9, and 3 km.

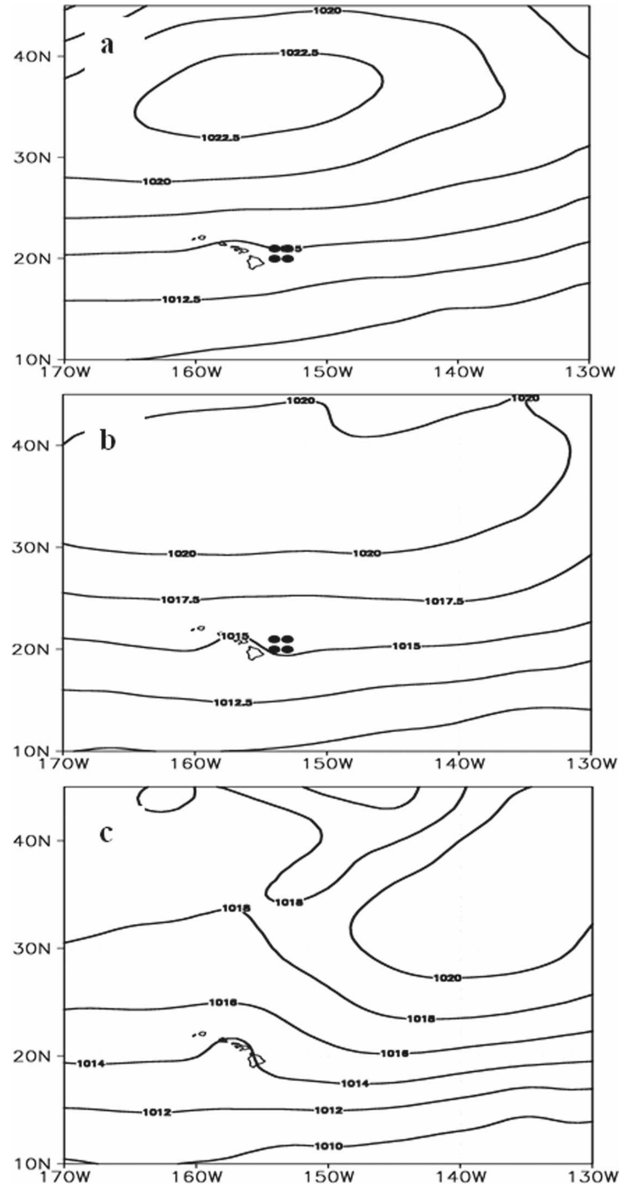

FIG. 2. The mean sea level pressure (hPa) from GFS analysis data at 0000 UTC, contour interval (CI) = 2.5 hPa, for (a) the eight strong and (b) the eight weak trade-wind days and for (c) the five southeasterly trade-wind days in the summer of 2004. The four dark points are used for the wind analysis in Table 1.

flow regimes (Smith 1989; Smolarkiewicz et al. 1988). Using a numerical model without surface friction and diabatic heating, Smolarkiewicz and Rotunno (1989) show that for Fr < 0.5, a pair of vertically oriented vortices is simulated on the lee side. For the island of Hawaii, the characteristic mountain height h is 3300 m (Carbone et al. 1998). With $N \sim 0.01\ \mathrm{s}^{-1}$, Fr varies from 0.3 for a strong trade-wind flow (10 m s^{-1}) to 0.15 for a weak trade-wind flow (5 m s^{-1}). In addition to Fr, the island-scale airflow and weather over the island of Hawaii are sensitive to trade-wind inversion height (Chen and Feng 1995; Chen and Feng 2001). With mountain heights ($>$4000 m) well above the typical height of trade-wind inversion ($\sim$2 km), the trade-wind inversion serves as a lid forcing the low-level flow on the windward side to split and move around the island (Leopold 1949; Chen and Feng 2001). The large wake off the leeside Kona coast with two large counterrotating vortices (Patzert 1969; Nickerson and Dias, 1981; Smith and Grubišić 1993) occurs in the flow regime because of the inability of the flow to move over the mountaintops of Mauna Loa and Mauna Kea (Schär and Smith 1993). In addition to the large wake off the Kona coast, a small wake also occurs off the leeside coast of the Kohala Mountains in northwest Hawaii (Smith and Grubišić 1993). The small wake occurs in the flow regime by transition to supercritical flow and the presence of a hydraulic jump over the lee slope for a small (Fr < 1)

TABLE 1. Statistics of the wind speed (m s^{-1}) and directions from GFS 1000 and 925-hPa level wind data at 0000 UTC at the four dark points upstream of the island of Hawaii in Fig. 2a for the eight strong and the eight weak trade-wind days and the five southeasterly (SE) trade-wind days.

	Max wind speed	Min wind speed	Mean wind speed	Max wind direction	Min wind direction	Mean wind direction
Strong	8.7	7.2	7.9	89°	65°	79°
Weak	5.9	4.1	5.2	88°	72°	80°
SE	9.0	5.1	7.1	130°	116°	121°

flow regime when the perturbation wind speed ($\sim Nh$) is relatively large when compared with U. Both flow regimes are associated with wakes that entail significant potential vorticity (PV) features and sometimes reversed flow. Potential vorticity results from a hydraulic jump or contact discontinuities related to the joining of two separate streams of fluid with different values of the Bernoulli function (Schär and Smith 1993).

Diabatic heating from orographic clouds and precipitation feeds back to the island-induced circulation affecting island-scale airflow and weather for the island of Hawaii (Chen and Feng 2001). Condensation heating and evaporative cooling affect flow transition, namely "flow over" and "flow around" a mesoscale mountain and atmospheric stratification (Buzzi et al. 1998; Miglietta and Buzzi 2001; Colle 2004; and others). Idealized simulations for a conditionally unstable flow over an idealized 2D mountain (Chu and Lin 2000; Chen and Lin 2005; and others) show that for a moist airflow over mountain barriers with clouds and precipitation, the unsaturated moist Froude number ($F_w = U/N_w h$, where U is the incoming wind speed, N_w is the moist Brunt–Väisälä frequency, and h is the maximum mountain height) and the convective available potential energy (CAPE) are two important control parameters for flow regimes For the trade-wind flow over the Hawaiian Islands, CAPE is about 100 J kg^{-1} within the trade-wind layer (~2 km) (Carbone et al. 1998; Li and Chen 1999), much smaller than in Chen and Lin (2005) (487–3578 J kg^{-1}), with a deep conditionally unstable atmosphere.

In addition to orographic blocking, the land surface processes can significantly affect the island-scale circulations throughout the diurnal cycle, especially in areas with weak surface winds due to orographic blocking or under a weak trade-wind flow (Leopold 1949; Chen and Nash 1994; and others). In the past, many numerical studies for the island of Hawaii have been conducted (Nickerson 1979; Fett and Bury, 1981; Smolarkiewicz et al. 1988; Rasmussen et al. 1989; Ueyoshi and Han 1991; Reisner and Smolarkiewicz 1994; and others); however, the diurnal thermal forcing from the land surface was crudely estimated in these studies.

Feng and Chen (2001) used the fifth-generation Pennsylvania State University–National Center for Atmospheric Research (NCAR) Mesoscale Model (MM5), version 1, to successfully simulate the nocturnal regime on the windward side of the island of Hawaii with the land surface specified as tropical rain forest over the entire island. Zhang et al. (2005a,b) coupled a mesoscale spectral model (MSM; Juang 2000) with an advanced land surface model (LSM) with high-resolution land surface parameters and simulated the sea-breeze circulations for a 6-day period over northwest Hawaii and the summer trade-wind weather over Oahu, with 3- and 1.5-km resolution, respectively. The initial soil moisture is specified based on ground cover. After the first day, the soil conditions (soil temperature and soil moisture) were updated from the 24-h output of the previous day's run. The MSM–LSM model was run for 1 month prior to the study period to incorporate the impact of orographic precipitation patterns on soil

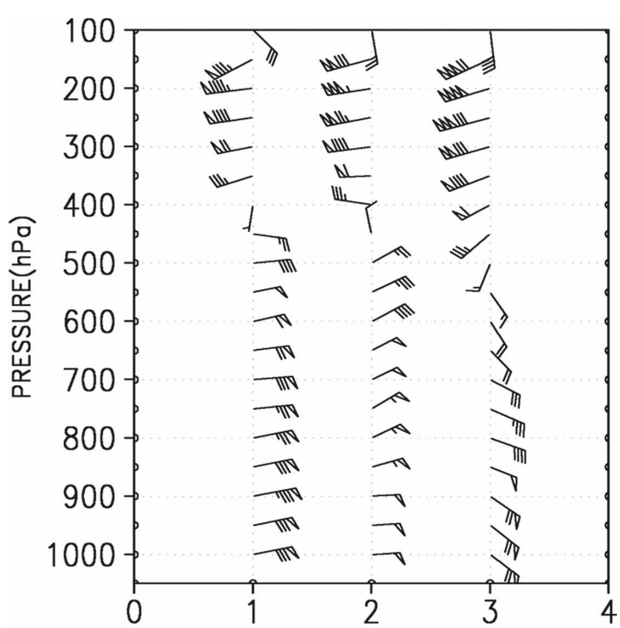

FIG. 3. Mean wind profiles calculated from winds at four dark grid points upstream of the island of Hawaii in Fig. 2 for the eight strong trade-wind days (column 1), the eight weak trade-wind days (column 2), and five southeasterly trade-wind days (column 3). Pennants, full barbs, and half barbs represent 5, 1, and 0.5 m s^{-1} respectively (the same hereinafter).

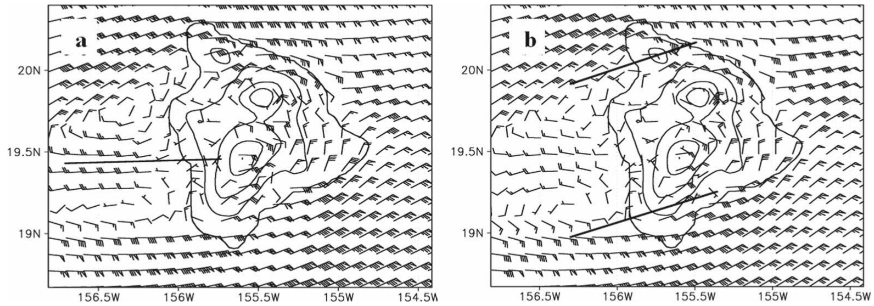

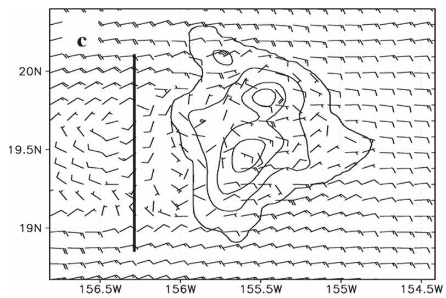

FIG. 4. Mean surface winds for (a) the eight strong and (b) the eight weak trade-wind days, and (c) their differences [(a) − (b)]. The thick solid lines show the locations of vertical cross sections used in the analyses.

moisture fields. Using MM5–LSM version 3 (Chen and Dudhia 2001), Yang et al. (2005) successfully simulated the island-scale circulations of the island of Hawaii throughout the diurnal cycle with improved surface parameters compiled by Zhang et al. (2005b). They validated their model results with Hawaiian Rainband Project (HaRP) data and showed that better surface conditions lead to better simulation of the strength of land and sea breezes. They also simulated the thermally direct circulation cells on both the windward side and the Kona lee side.

For the island of Hawaii, observation studies showed pronounced variations of local winds and weather under different trade-wind strength. The inland advance of sea breezes in the afternoon in the lee side of the Waimea Saddle of northwest Hawaii is more significant under weak trade-wind flows (Schroeder 1981; Yang and Chen 2003, hereinafter YC03). Chen and Nash (1994) showed that the onset times of the downslope/offshore and upslope/onshore flow depend on the strength of the prevailing trade-wind flow. YC03 showed that the adiabatic descent of trade-wind flow aloft on the northwestern and southwestern lee sides of the island of Hawaii is more significant with less rainfall for a strong trade-wind flow. However, in previous numerical studies, the effects of the trade-wind strength and direction on the leeside circulations and weather throughout the diurnal cycle were not studied in detail. The island of Maui was not included in most of these modeling studies except in Yang et al. (2005), Yang and Chen (2008), and Zhang et al. (2005b), resulting in an underestimation of the strength of the airflow passing

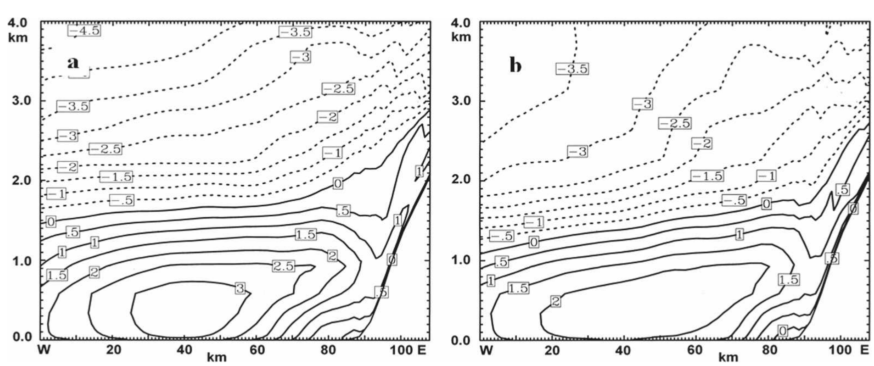

FIG. 5. Height–distance cross sections of the mean zonal wind speed along the westerly reversed flow in Fig. 4a, CI = 0.5 m s^{-1}, for (a) the eight strong and (b) the eight weak trade-wind days.

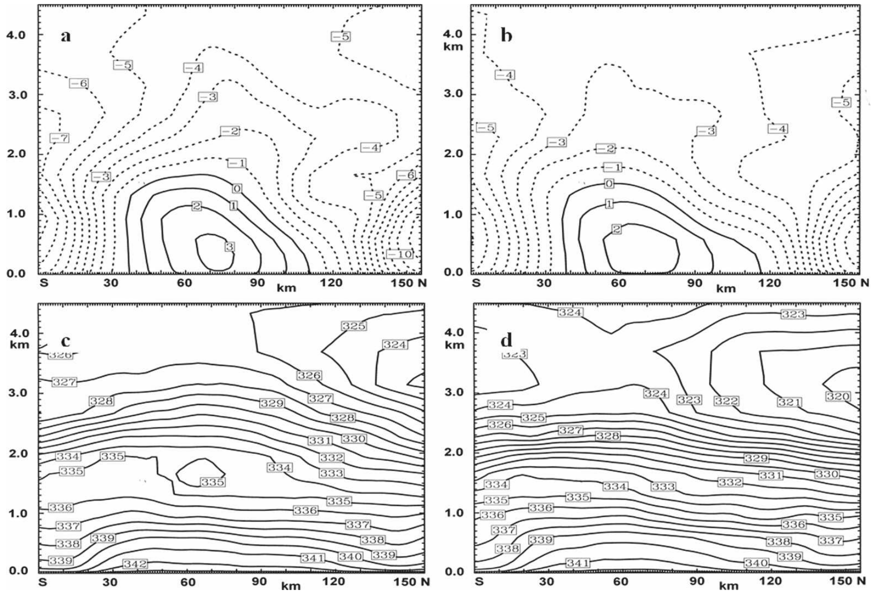

FIG. 6. Height–distance cross sections across the westerly reversed flow (the solid line in Fig. 4c). (a), (b) Daily mean zonal wind speed, CI = 1 m s^{-1}, for (a) the eight strong and (b) the eight weak trade-wind days. (c), (d) Daily mean equivalent potential temperature, CI = 1 K, for (c) the eight strong and (d) the eight weak trade-wind days.

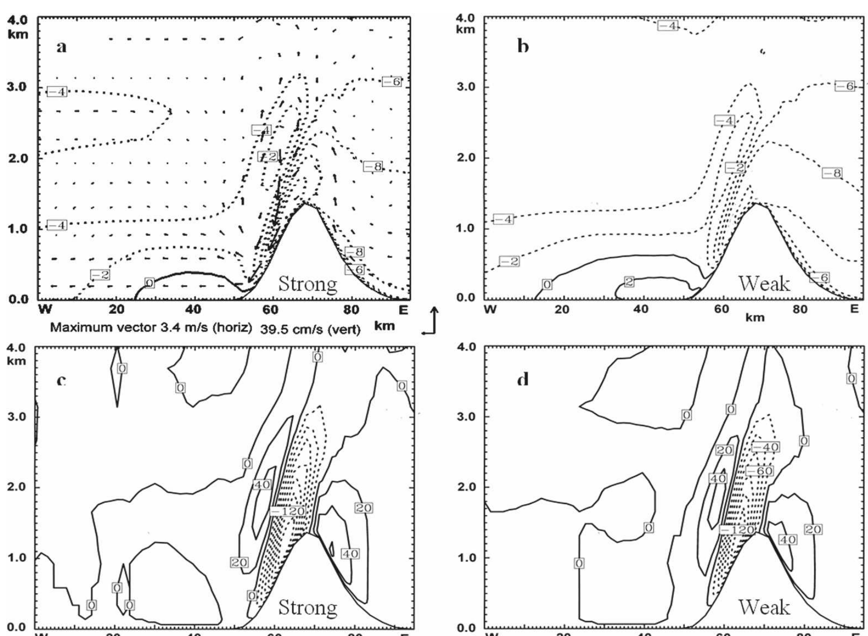

FIG. 7. Height–distance cross sections along the trade-wind flow in the northern area of the island (Fig. 4b). (a), (b) The mean wind speed, CI = 2 m s^{-1}, for (a) the eight strong and (b) the eight weak trade-wind days. (c), (d) The mean vertical velocity, CI = 20 cm s^{-1}, for (c) the eight strong and (d) the eight weak trade-wind days. Vector differences of winds between the eight strong and the eight weak trade-wind days are shown in (a) with vector scales shown at the bottom of (a).

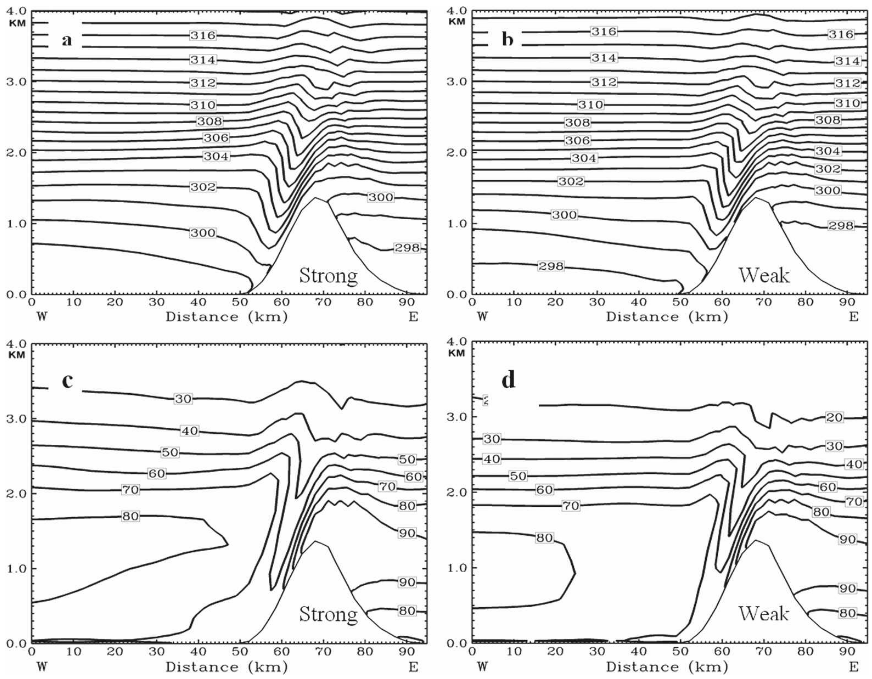

FIG. 8. (a), (b) Height–distance cross sections of the mean potential temperature with an interval 1 K and (c), (d) the mean RH (%), CI = 10%, along the trade-wind flow in the northwestern area of the island (Fig. 4b) for (a), (c) the strong trade-wind days and (b), (d) the weak trade-wind days.

through the Alenuihaha Channel between the island of Maui and the island of Hawaii.

Over the northwestern and southwestern leeside areas, hydraulic jumps may occur with significant potential vorticity generation (Smith and Grubišić 1993). How does the trade-wind speed affect the hydraulic jumps and airflow there? How does the diurnal heating cycle modify the simulated circulations on the lee side?

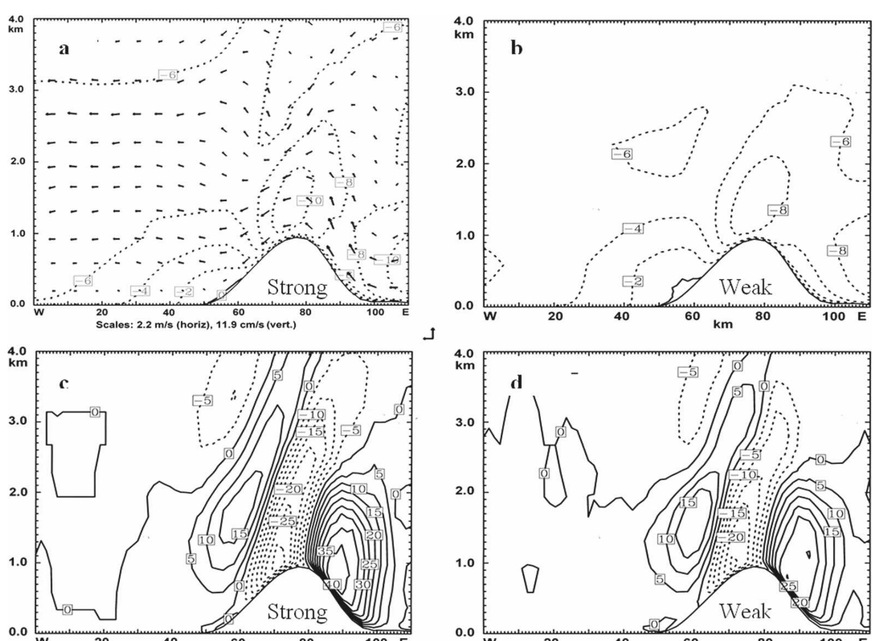

FIG. 9. As in Fig. 7, but for the southern area of the island (Fig. 4b). The CI for the vertical velocity is 5 cm s^{-1}. Vector scales are shown at the bottom of (a).

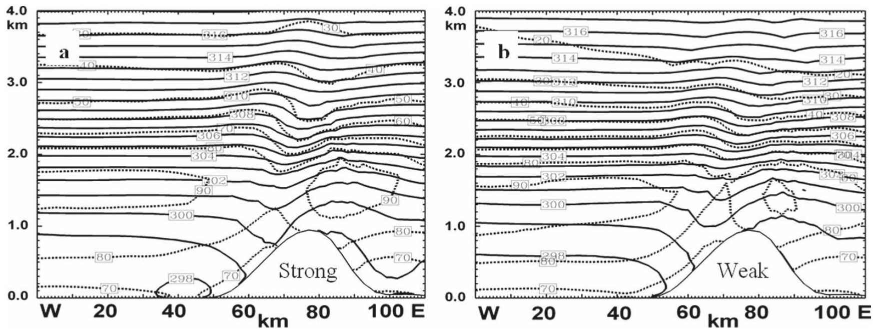

FIG. 10. Height–distance cross sections of the mean potential temperature (solid lines) with an interval of 1 K and the mean RH (%, dotted lines), CI = 10%, along the trade-wind flow in the southern area of the island (Fig. 4b) for (a) the strong and (b) the weak trade-wind days.

How does the trade-wind speed affect the strength of the offshore westerly return flow for the small wake off northern Hawaii and the large wake off the Kona coast? Along the Kona leeside coastal area, an evening rainfall maximum during the diurnal cycle was found from the analysis of data collected during the Hawaiian Rainband Project (11 July–24 August 1990; Chen and Nash 1994). For the strong trade-wind days, the rainfall maximum there is greater than for the weak trade-wind days (YC03). On the other hand, evening rainfall along the Kona coast is not sensitive to the observed trade-wind inversion height observed by Hilo soundings (Chen and Feng 1995). YC03 speculated that the enhanced convergence between the land breezes and a stronger and moist reversed flow offshore is the possible reason for the greater rainfall production in the evening there when trades are stronger. However, few observational data were collected off the Kona leeside coast during HaRP. This problem will be investigated in this study using a numerical model.

The trade-wind direction also affects the leeside circulations and rainfall production. For the island of Hawaii, with a more northerly wind direction, the wake circulation is dominated by a cyclonic lee vortex (Rasmussen et al. 1989). During the approach of a midlatitude cold front to the north, winds over the Hawaiian Islands frequently turn to southeasterlies. A southeasterly airflow would face a wider mountain ridge than a normal trade-wind flow (Rasmussen et al. 1989). Numerical simulations with an idealized bell-shaped mountain showed that for a wider mountain, the leeside circulations would be wider and deeper (Smolarkiewicz and Rotunno 1989; and others). However, the leeside circulations and rainfall throughout the diurnal cycle for the island of Hawaii under a southeasterly trade-wind flow have not been studied.

The objective of this study is to investigate the effects of trade-wind strength (strong trade-wind flow versus weak trade-wind flow) and direction (southeasterly flow versus normal trade-wind flow) on the circulation, thermal field, and rainfall production on the leeside of the island of Hawaii and to determine how the land surface thermal forcing throughout the diurnal cycle modifies these effects. In this study, the high-resolution (3 km) simulations of MM5/LSM over the island of Hawaii during the summer of 2004 were used.

2. Model description and initialization

The MM5 (Dudhia 1993) is a nonhydrostatic, three-dimensional primitive equation model employing the terrain-following sigma vertical coordinate. In this study, there are 29 sigma levels[1] from the surface to the 100-hPa level. Four nested domains with two-way nesting were used to simulate the island-induced circulations over the island of Hawaii, with horizontal resolutions of 81, 27, 9, and 3 km, respectively (Fig. 1b). Grell's cumulus parameterization (Grell 1993), a grid-scale warm rain process (Hsie et al. 1984), a cloud radiation scheme (Dudhia and Moncrieff 1989), and Hong and Pan's (1996) boundary layer scheme are used in the model. The LSM module has four layers at depths of 10, 40, 100, and 200 cm (Chen and Dudhia 2001). The land use, soil type, and vegetation fraction over the island of Hawaii are from Zhang et al. (2005b).

The daily MM5–LSM experimental runs have been conducted since the early fall of 2003 for the island of Hawaii with soil moistures and soil temperatures updated from the 24-h simulation of the previous day. The simulations are initialized by the National Centers for Environmental Prediction (NCEP) Global Forecasting

[1] The full sigma levels are 1.0, 0.999, 0.996, 0.993, 0.990, 0.984, 0.980, 0.96, 0.925, 0.865, 0.82, 0.79, 0.76, 0.73, 0.7, 0.67, 0.64, 0.60, 0.55, 0.50, 0.45, 0.41, 0.36, 0.31, 0.26, 0.21, 0.16, 0.1, 0.05, and 0.0.

System (GFS) 1° × 1° data at 0000 UTC. The simulation procedures are the same as Yang et al. (2005), except that in these studies NCEP–NCAR reanalysis is used to provide initial and lateral boundary conditions. In this study, we use the output of MM5–LSM from 15 July to 31 August during summer 2004. The model daily hourly output during the 12th–35th-hour simulation (or from 1200 UTC to 1100 UTC the next day) is used to represent the simulated diurnal cycles. The simulated diurnal cycles are not sensitive to the model initialized time.

For summer 2004, the mean upstream wind speed and direction at 0000 UTC (i.e., the 24th hour of model simulation time) for each day from 15 July to 31 August are computed by using the wind data from the four dark grid points (Fig. 2) at both the 1000- and 925-hPa levels. From the computed mean upstream wind speed and direction at 0000 UTC, a strong trade-wind day is classified if the mean wind speed is higher than 7 m s^{-1} with a wind direction between 60° and 90°. The eight strongest trade-wind days (16, 17, and 29 July; 7, 16, 24, 25, and 28 August) are identified from these criteria, with a mean wind speed and wind direction of 7.9 m s^{-1} and 79°, respectively (Table 1). The eight weakest trade-wind days (18, 19, 22, and 30 July; 15, 20, 29, and 30 August) are also identified from the weakest mean wind speed, with a wind direction between 60° and 90°. The mean wind speed and direction of the eight weak trade-wind days are 5.2 m s^{-1} and 80°, respectively. Twelve hours earlier at 0000 UTC [0200 Hawaiian standard time (HST)], the strong and weak trade-wind days have mean wind speeds of 8 and 5.7 m s^{-1}, respectively. For the strong trade-wind days, the composite subtropical high is to the north of the Hawaiian island chain (Fig. 2a). For the weak trade-wind days, a midlatitude cold front is present to the north of the Hawaiian island chain, with a weaker subtropical high (Fig. 2b). From the daily 0000 UTC Hilo sounding on the windward side of the island of Hawaii, the inversion height varied from 1900 to 2400 m for the eight strong trade-wind days with a mean of 2100 m, and from 1600 to 2050 m for the eight weak trade-wind days with a mean height of 1850 m.

Five days (20 July; 4, 8, 18, and 19 August) with a wind direction at low levels between 110° and 130° are classified as southeasterly trade-wind days. The mean wind direction and wind speed for these five days are 121° and 7.1 m s^{-1}, respectively (Table 1). For the five days with a southeasterly flow, the subtropical high is split into two highs by the approach of a midlatitude cold front from northwest of the Hawaiian island chain. The high to the northeast of the Hawaiian island chain has a larger surface pressure maximum than the high to the northwest of the island chain (Fig. 2c). The composite geopotential heights at the 500-hPa level for the five days with a southeasterly flow (not shown) exhibit a deeper trough along 152°W than for the weak trade-wind days.

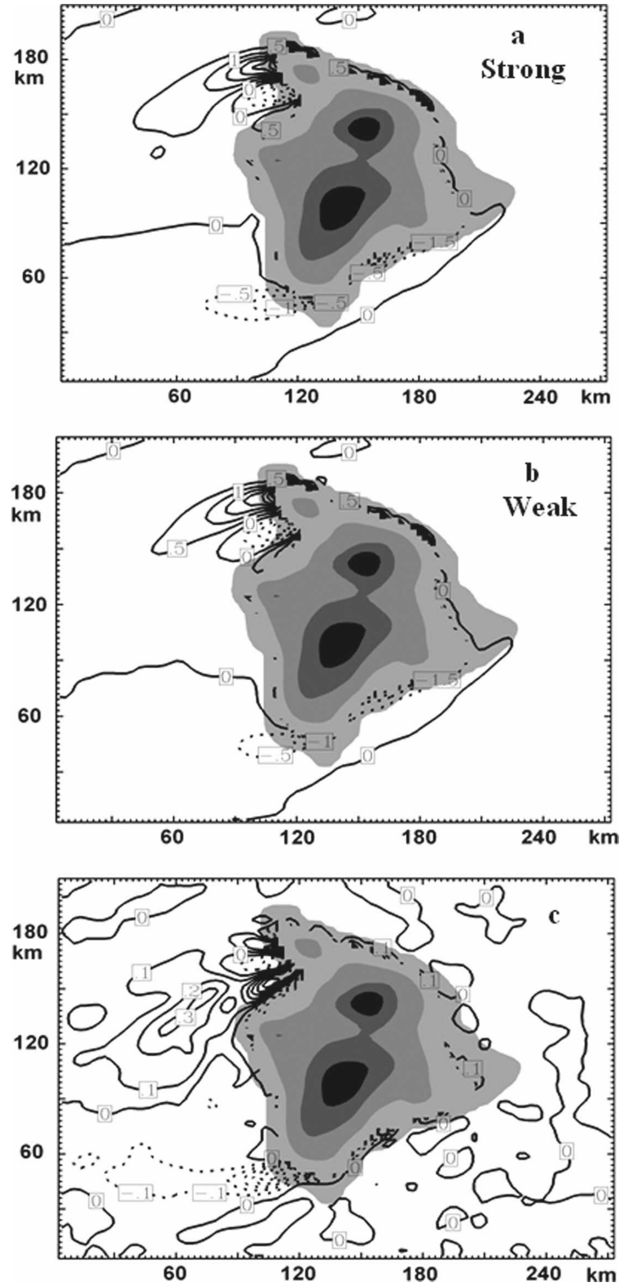

FIG. 11. The mean potential vorticity (PVU; 1 PVU = 10^{-6} K m^2 s^{-1} kg^{-1}) at 500 m MSL, CI = 0.5 PVU, for (a) the eight strong and (b) the eight weak trade-wind days. (c) The differences between (a) and (b), CI = 0.1 PVU.

For the strong and the weak trade-wind days (Fig. 3), the top of the northeasterly flow upstream of the island

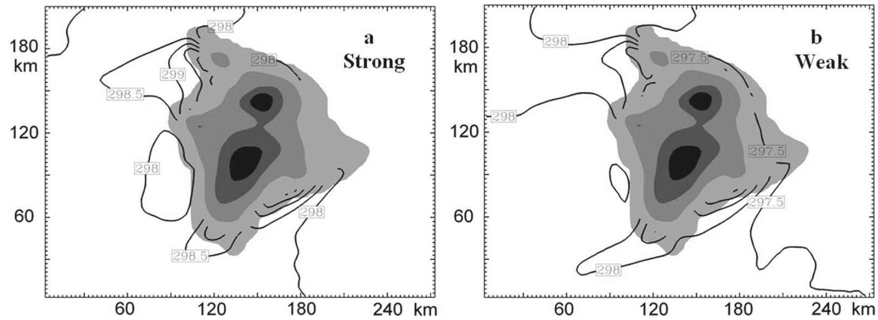

FIG. 12. The mean potential temperature, CI = 0.5 K, for (a) the eight strong and (b) the eight weak trade-wind days at 500 m MSL.

of Hawaii is at the 350–400-hPa level. Below the 400-hPa level, the mean wind speed for the strong trade-wind days is 3 m s^{-1} greater than for the weak trade-wind days. The top of the southeasterly flow regime is at the 450-hPa level. At low levels, the wind speed of the southeasterly flow regime is 1 m s^{-1} less than the strong trade-wind days and 2 m s^{-1} greater than the weak trade-wind days. At high levels, the westerly winds are the strongest for the southeasterly flow regime. For the low-level temperature profiles (not shown), the air temperature is slightly higher (~0.2 K) for the southeasterly flow than for strong and weak trade-wind days. The air temperatures below the 850-hPa level for the strong and weak trades are almost the same with $N \sim 0.01$ s^{-1}. For $h \sim 3$ km, Fr is ~0.27 and 0.17 for the strong and weak trade-wind cases, respectively.

3. Effects of trade-wind strength

In this section, the differences of the mean lee-side circulations, the mean thermal fields, and total rainfall accumulation between the eight strong and the eight weak trade-wind days during summer 2004 were studied using the hourly model data for these days.

a. Mean state

1) WAKE CIRCULATIONS

The southeasterly (northeasterly) winds along the northeastern (southeastern) coast, easterly winds around the southern and northern tips of the island, and winds through the Waimea and the Humu'ula Saddle are 1.5–2.5 m s^{-1} stronger when trades are

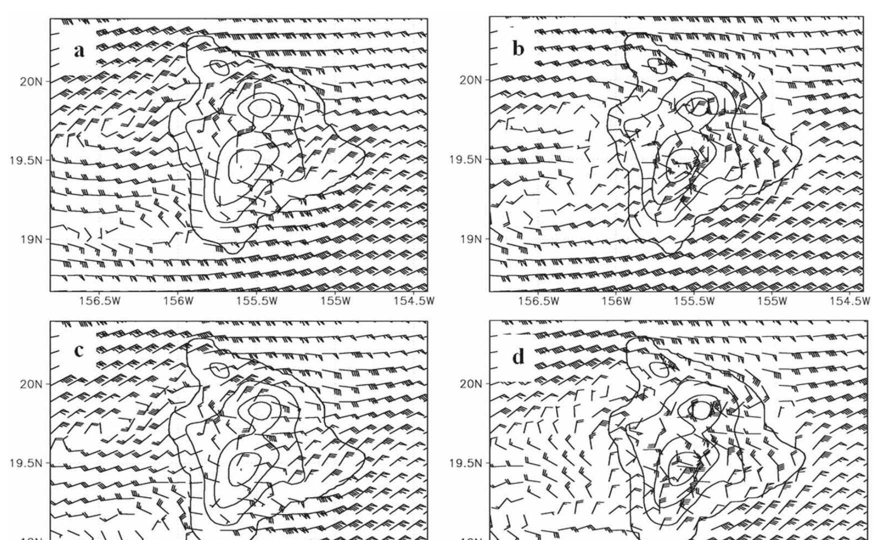

FIG. 13. The mean surface winds for (a), (b) the eight strong trade-wind days at (a) 1400 and (b) 0500 HST and (c), (d) the eight weak trade-wind days at (c) 1400 and (d) 0500 HST.

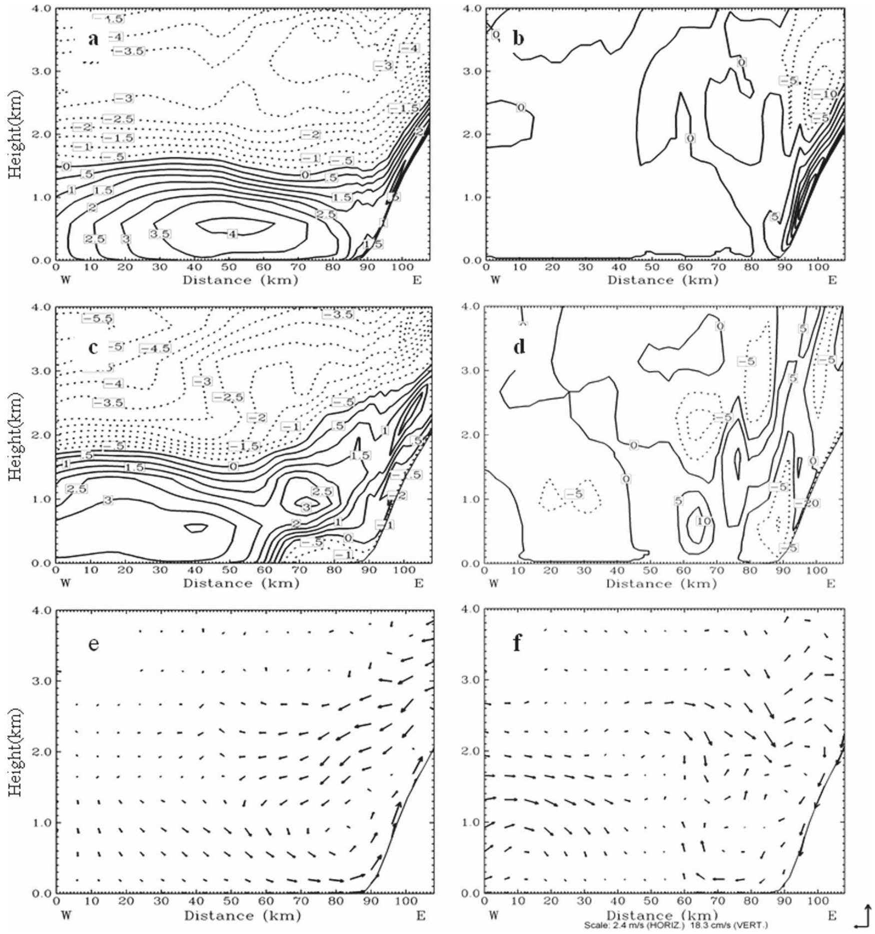

FIG. 14. Height–distance cross sections along the westerly reversed flow of the large wake (the solid line in Fig. 4a) for the eight strong trade-wind days. (a), (c) The mean zonal wind speed, CI = 0.5 m s^{-1}, at (a) 1400 and (c) 0500 HST; (b), (d) the mean vertical velocity, CI = 5 cm s^{-1}, at (b) 1400 HST, and (d) 0500 HST; and (e), (f) vectors of wind deviations from the daily mean at (e) 1400 and (f) 0500 HST. Vector scales are shown in Fig. 15f.

stronger (Fig. 4). Flow separation occurs on the windward lower slopes, with a westerly return flow in the large wake zone for both the strong and weak trade-wind days, as a result of the inability of the flow to move over high mountaintops with tops well above the trade-wind inversion (Schär and Smith 1993; Chen and Feng 2001). For a stronger incoming trade-wind flow, the flow splitting on the windward side is more significant (Chen and Nash 1994), with a stronger (3 versus 2 m s^{-1}) and deeper (200–300 m) westerly reversed flow off the leeside Kona coast (Figs. 4 and 5). The deeper westerly reversed flow for the stronger trade-wind days may be related to the fact that the trade-wind inversion is higher for the strong trade-wind days than the weak trade-wind days (2100 versus 1850 m). The nondimensional westerly reversed wind speed (u/U) is about the same (0.4) for both cases.

The maximum easterly winds at the northern and southern ends of the north–south cross section (Fig. 4c) are 2–4 m s^{-1} greater for the strong trade-wind days than for the weak trade-wind days (Figs. 6a,b). The maximum differences are greater than the differences of the upstream trade-wind speeds between the strong and weak trade-wind cases. The leeside counterrotating vortices are more significant when trades are stronger (Fig. 4). At low levels, the equivalent potential temperature (Figs. 6c,d) within the westerly reversed flow along the axis of counterrotating vortices is higher than at the northern and southern ends of the north–south cross section. The westerly reversed flow is a weak convergence zone with a weak rising motion (1–2 cm s^{-1}; not shown) that is slightly stronger with slightly higher equivalent potential temperatures when trades are stronger (Figs. 6c,d).

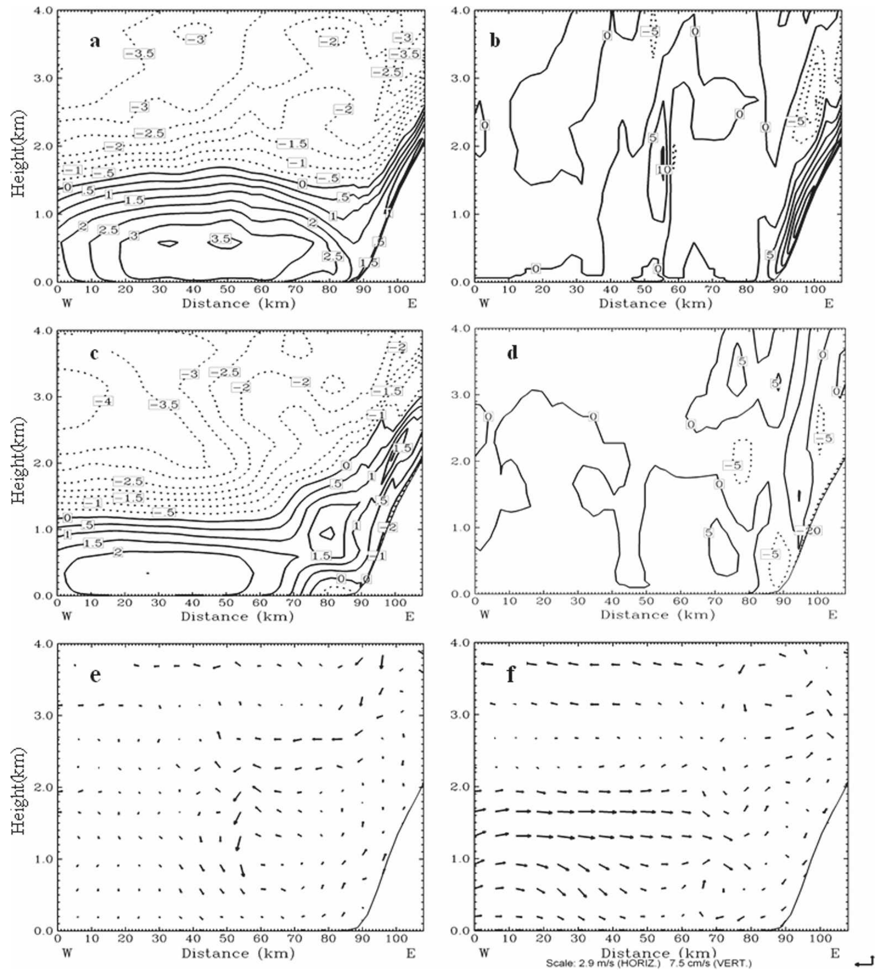

FIG. 15. As in Fig. 14, but for the eight weak trade-wind days.

2) WINDS OVER THE NORTHWESTERN AND SOUTHWESTERN LEESIDE AREAS

For the Kohala Mountains over northern Hawaii with summits (1700 m) below the trade-wind inversion, the trade-wind flow aloft can move over the mountain tops. The simulated mean airflow upstream has wind speeds (U) of 11 and 8 m s^{-1} for the strong and weak trade-wind days, respectively. With $N \sim 0.01$ s^{-1}, Fr is 0.7 and 0.48 for the strong and the weak trade-wind flows, respectively. For both the strong and weak trade-wind cases, the flow regime for northern Hawaii is characterized by lee vortices with a reversed flow between them (Figs. 4 and 7). For the strong trade-wind days, the reversed flow in the small wake is weaker than for the strong trade-wind days (0.5 versus 2.5 m s^{-1} or $u/U \sim 0.05$ versus 0.3; Figs. 7a,b) in agreement with Smolarkiewicz and Rotunno (1989). This is in contrast to the return flow of the large wake off the central Kona leeside coast, where the return flow is stronger when trades are stronger. Significant downslope winds occur on the leeside slopes of the Kohala Mountains (Fig. 7). As the trade-wind flow moves over the mountains, the incoming flow continue to accelerate with decreasing depth of the warm, moist trade-wind layer (Fig. 8) until the flow becomes supercritical over the lee slopes followed by a jump (because the flow must return to subcritical downstream; Schär and Smith 1993). For the strong trade-wind days, the horizontal wind speed decreases from 13 m s^{-1} ($u/U \sim 1.2$) over the mountaintop and the leeside upper slopes to 2 m s^{-1} ($u/U \sim 0.2$) within a distance of 15 km downstream (Fig. 7a), whereas for the weak trade-wind days it decreases from 10 ($u/U \sim 1.3$) to 2 m s^{-1} ($u/U \sim 0.3$; Fig. 7b). The maximum sinking motion associated with the downslope winds are 1.5 and 1.2 m s^{-1} for the strong and the weak trade-wind days (Figs. 7c,d), respectively. The abrupt decrease in horizontal wind speed is accompanied by rising motion. The maximum rising motion is 0.4 m s^{-1} for both the strong and the weak trade-wind days (Figs. 7c,d). The leeside downslope flow is 3–4 m s^{-1} stronger for the strong trade-wind days than for the weak trade-wind days (Figs. 7a,b).

For the cross section over northwest Hawaii (Fig. 8), the isentropic surfaces (Figs. 8a,b) above the mountain tops descend to lower levels immediately downstream of the Kohala Mountains, accompanied by a sharp drop in the relative humidity (Figs. 8c,d). The descent of the isentropic surfaces and the drop in the relative humidity for the strong trade-wind days are more significant than for the weak trade-wind days. Immediately downstream, the isentropic surfaces tilt upward and are accompanied by an increase in the relative humidity.

Over the southwest leeside slope (Figs. 9 and 10), a hydraulic jump is also simulated where the southern branch of the splitting airflow moves along the southwestern coast over the southern end of the ridge axis of Mauna Loa. The variations of the horizontal wind speed and the vertical motions associated with the hydraulic jump there are weaker than over the leeside slopes of the Kohala Mountains. When trades are stronger, the hydraulic jumps over the northwestern and southwestern leeside areas are more significant.

Positive PV mainly occurs on most of the northwestern leeside area with a maximum on the leeside slopes of the Kohala Mountains. Near the positive PV maximum is a negative PV maximum on the leeside slope close to the Waimea Saddle (Fig. 11). To the south of the negative PV is another positive PV maximum, with positive PVs emanating downstream from there. Larger negative PVs are simulated on the southwestern leeside areas. The negative PVs in the southwestern leeside areas are produced by contact discontinuities (Schär and Smith 1993). The PV anomaly patterns on the northwestern leeside are produced by a combination of hydraulic jump on the leeside slopes of the Kohala Mountains and contact discontinuities between the flow around the island and the larger wake. The hydraulic jump on the leeside slopes is accompanied by downstream advection of positive (negative) PVs over the northern (southern) leeside areas (Schär and Smith 1993).

For the strong trade-wind days, the negative PV in the southwestern leeside area and the positive PV in the northwestern leeside area are larger than those for the weak trade-wind days (Fig. 11c) as a result of significant wind shear in these regions for the strong trade-wind days (Fig. 4c). With larger PV production for the strong trade-wind days, the large wake circulation is more pronounced with stronger westerly return flow (Fig. 4).

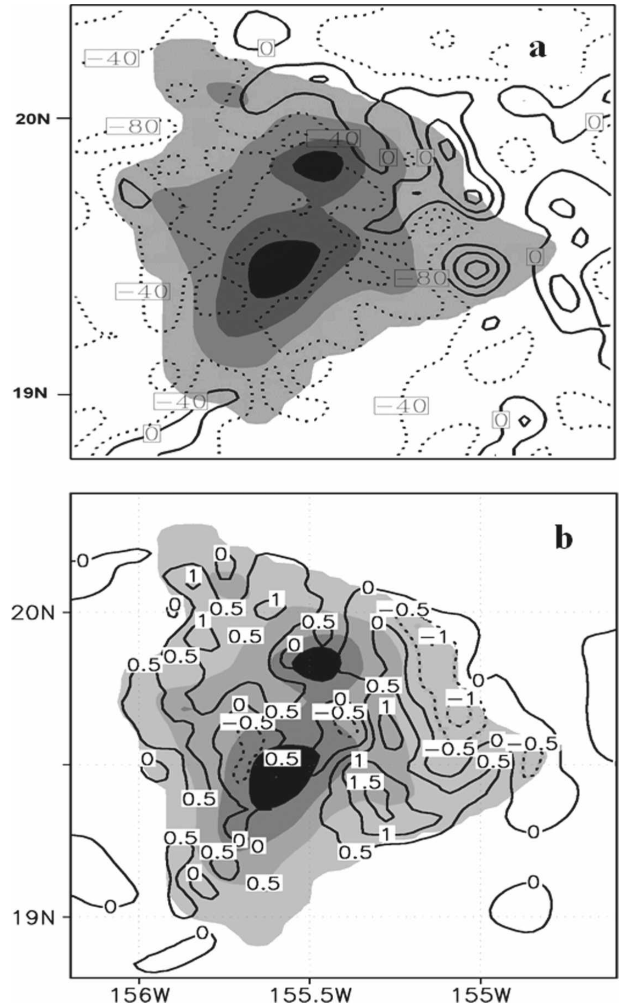

FIG. 16. (a) Differences of the mean integrated cloud water content (10^{-3} mm) and (b) differences of the mean surface air temperature between the eight strong and the eight weak trade-wind flow days at 1400 HST.

3) Horizontal distribution of thermal fields

For both the strong and weak trade-wind days in summer 2004 (Fig. 12), maximum temperatures are simulated on the southwestern and northwestern lee sides, as well as on the lee side of the Kilauea volcanoes in the southeastern area of the island, consistent with observational studies (Chen and Wang 1994; Smith and Grubišić 1993; YC03). For the strong trade-wind days (Fig. 12a), the temperature maximum on the northwestern and southwestern leeside areas of the island are 0.5–1 K higher than for the weak trade-wind days (Fig. 12b). It is apparent that a stronger trade-wind flow results in a stronger descending trade-wind flow aloft with more significant adiabatic warming over these areas.

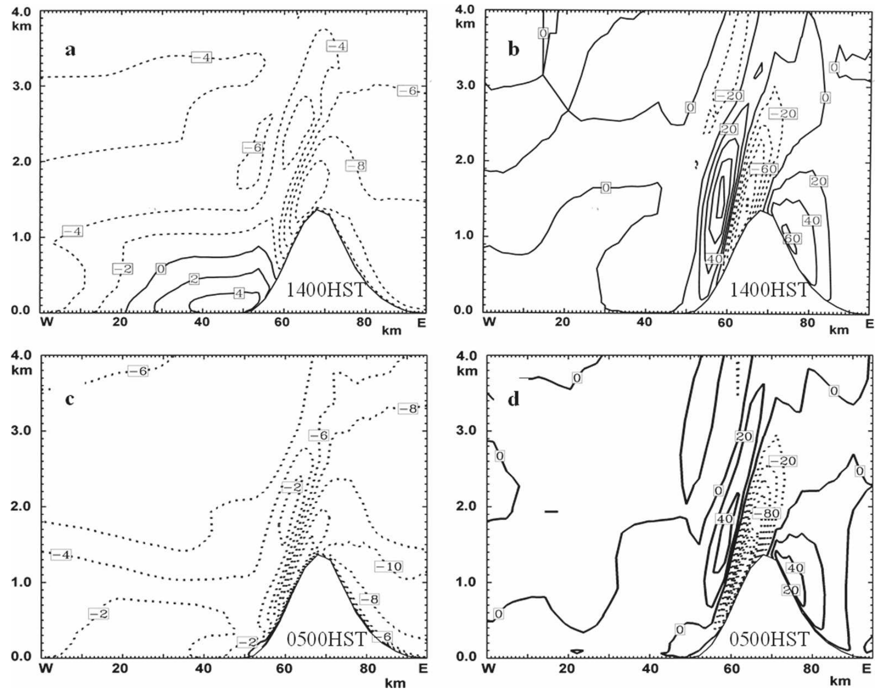

FIG. 17. Height–distance cross sections along the trade-wind flow over the northwestern area of the island of Hawaii (Fig. 4b) for the eight strong trade-wind days. (a), (c) The mean wind speed, CI = 1 m s^{-1}, at (a) 1400 and (c) 0500 HST and (b), (d) the mean vertical velocity, CI = 20 cm s^{-1}, at (b) 1400 and (d) 0500 HST.

These features are consistent with the results from the analyses of portable automatic mesonet data during HaRP (YC03).

b. Daytime and nighttime regimes

In this section, we investigate how the variations of the wake circulations—hydraulic jumps over the northwest and southwest leeside slopes under strong and weak trade-wind flows—are modified by the daytime heating and nighttime cooling at the land surface. We use data at 1400 and 0500 HST to represent the daytime and nighttime regimes, respectively.

1) LEESIDE CIRCULATIONS

During the daytime, over the ocean off the Kona coast, the westerly reversed flow in the large wake zone is enhanced by merging with the sea breezes along the coast (Fig. 13a). The wind speed difference of the westerly reversed flow offshore between the strong and the weak trade-wind days is only 0.5 m s^{-1} in the afternoon (Figs. 13a,c), 0.5 m s^{-1} smaller than the mean state difference (1 m s^{-1}; Fig. 4).

Over the Kona slopes, anabatic winds develop at low levels with the combined return branch of the anabatic flow and trade-wind flow aloft in the afternoon hours (Figs. 14a and 15a). For the strong trade-wind days, the descending trade-wind flow moving from the Humu'ula Saddle between Mauna Loa and Mauna Kea and high mountain ridges aloft has a stronger (5–10 cm s^{-1}) sinking motion than for the weak trade-wind days (Fig. 15e) with less cloud cover (Fig. 16a). In addition to trade-wind strength, the trade-wind inversion height could affect the leeside circulations and weather. Observations and simulations (Chen and Nash 1994; Yang and Chen 2008; and others) show strong winds channeling through the gap between Mauna Loa and Mauna Kea. Furthermore, unlike the strong trade-wind days, for most of the weak trade-wind days, the trade-wind inversion (~1850 m) is below the model terrain of the Humu'ula Saddle (~2000 m), preventing the trade-wind flow from penetrating the inversion and moving through the saddle to descend in the lee. Therefore, land surface heating is more significant with higher surface air temperatures (Fig. 16b) when trades are stronger. The upslope flow is stronger (0.5 m s^{-1}), with a larger vertical shear between the upslope flow above the surface and easterly winds aloft, for the strong trade-wind days than for the weak trade-wind days; the onshore flow and the compensating sinking motion over the ocean off the Kona coast are also stronger

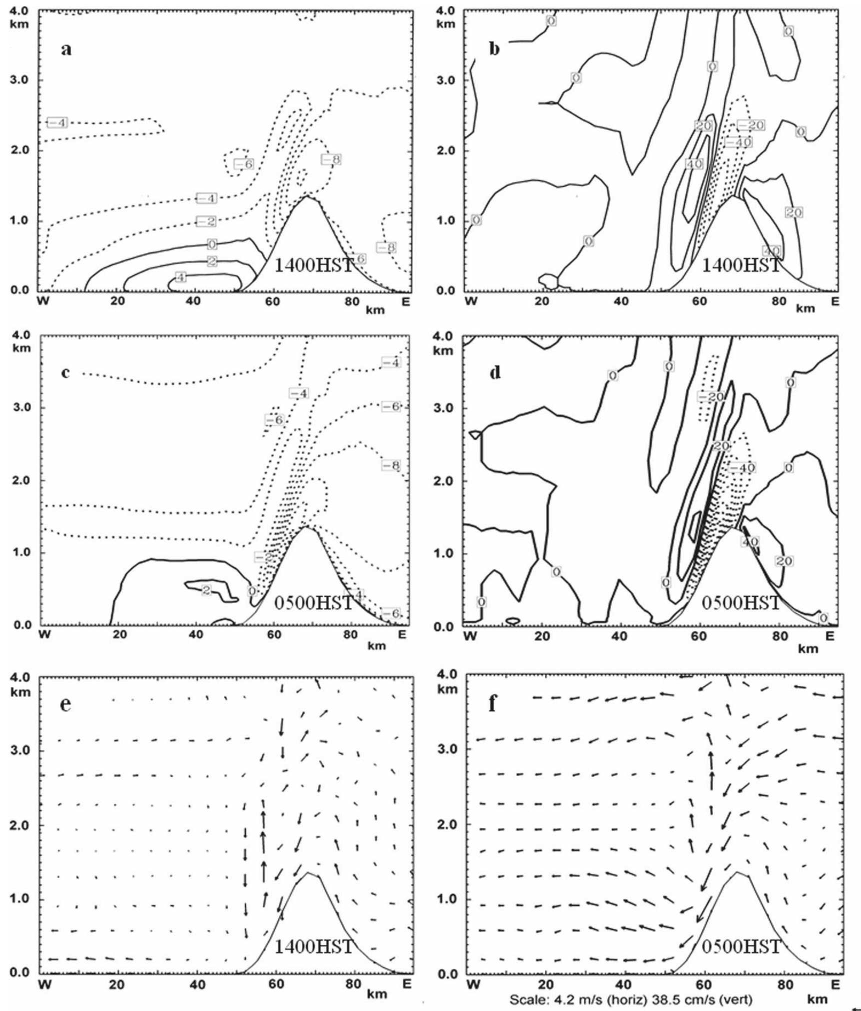

FIG. 18. Height–distance cross sections along the trade-wind flow in the northwestern area of the island (Fig. 4b) for the eight weak trade-wind days. (a), (c) The mean wind speed, CI = 1 m s^{-1}, at (a) 1400 and (c) 0500 HST; (b), (d) the mean vertical velocity, CI = 20 cm s^{-1}, at (b) 1400 and (d) 0500 HST; and (e), (f) vectors of wind differences between the eight strong and the eight weak trade-wind days at (e) 1400 and (f) 0500 HST. Vector scales are shown at the bottom of (f).

(Fig. 15e). The thermally direct circulation cell in the afternoon is more significant for the strong trade-wind days than for the weak trade-wind days (Fig. 15e).

At night, the westerly reversed flow offshore converges with the offshore/land-breeze flow over the Kona coastal region with katabatic flow on the Kona slopes (Figs. 13b,c) (Yang and Chen 2008). The westerly reversed flow at night is stronger (3.5 versus 2 m s^{-1}) for the stronger trade-wind days than for the weak trade-wind days (Figs. 14c and 15c), resulting in stronger rising motions (5–10 cm s^{-1}) with higher rainfall there (as will be shown in section 3c). For the strong trade-wind days, the downslope/offshore flow over the Kona coastal region is stronger (0.5–1 m s^{-1}) than the weak trade-wind days (Fig. 15f), perhaps a result of the feedback of the latent heat release of greater rainfall amount at night in this area.

2) WINDS OVER THE NORTHWESTERN AND SOUTHWESTERN AREAS

During the daytime, both the strong and weak trade-wind days are characterized by a westerly flow in the wake (Figs. 17a and 18a). Furthermore, the westerly flow in the wake merges with sea breezes along the leeside coast. The convergence between the descending trade-wind flow and the anabatic flow enhances the rising motions associated with the hydraulic jump aloft (Figs. 17b and 18b). As a result, the maximum rising motions over the leeside lower slopes of the Kohala Mountains in the afternoon are stronger (10–40 cm s^{-1}) than the daily mean (Figs. 7c,d). Furthermore, the rising motion is greater when trades are stronger (Fig. 18e).

At night, land surface cooling results in positive surface pressure perturbation (not shown) and the development of katabatic flow on the leeside slopes of the Kohala Mountains. The descending trade-wind flow aloft on the leeside upper slopes of the Kohala Mountains is enhanced by the katabatic flow (Figs. 17c,d and 18c,d), resulting in stronger downslope flow with larger (2–3 m s^{-1}) wind speed maximum and stronger sinking motions (20–30 cm s^{-1}) over the leeside slopes than the daily mean. For the strong trade-wind days, the combined downslope/katabatic flow prevails in the lee at night without a westerly reversed flow offshore.

Figures 18e and 18f show the differences of winds between the strong and weak trade-wind days in the afternoon and at night, respectively. For both the daytime and nighttime flow regimes (Figs. 18e,f), the orographic lifting on the upper windward slopes, the descending downslope winds past the mountaintops, and the rising motion associated with the jump are more significant when trades are stronger. However, the differences in westerly onshore flow in the afternoon along the leeside coast are relatively small between the strong and weak trade-wind cases (Figs. 17a and 18a,e) suggesting that the land surface heating over the semiarid lava rocks plays an important role in the development of the westerly flow under the opposing descending trade-wind flow (Zhang et al. 2005b). At night, with land surface cooling, the combined downslope/katabatic winds are 2–4 m s^{-1} stronger and extend farther down to the leeside coast when trades are stronger (Figs. 17c and 18c,f), resulting in a change from a flow regime with a weak reversed flow for the weak trade-wind days to a flow regime without a reversed flow for the strong trade-wind days.

c. Rainfall

For both the strong and the weak trade-wind days in summer 2004, rainfall accumulation on the windward side is greater than on the lee side (Fig. 19). On the windward lowlands, more rainfall occurs for the strong trade-wind days with the maximum rainfall axis farther inland than for the weak trade-wind days, which is consistent with observations (Esteban and Chen 2008). Over the central Kona coastal region on the lee side of the island, rainfall is greater (50 mm) for the strong trade-wind days than for the weak trade-wind days (Figs. 19a,b) in agreement with YC03.

In the central Kona coastal region and lower slopes,

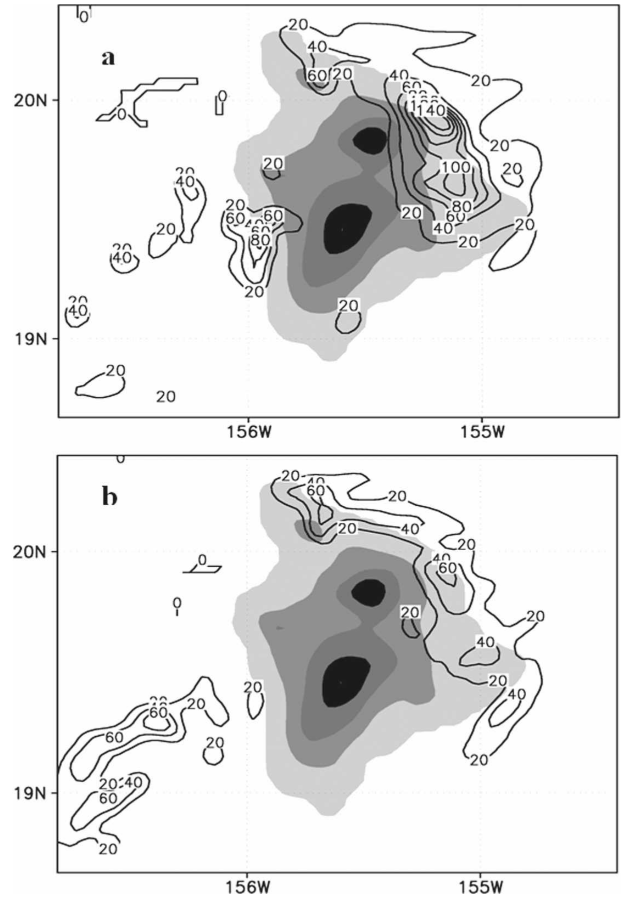

FIG. 19. The rainfall accumulation, CI = 20 mm, for (a) the strong and (b) the weak trade-wind days.

more rainfall occurs in the evening (Fig. 20) than in any other 4-h period due to the convergence between the westerly reversed flow offshore and the katabatic flow (Yang and Chen 2008). The maximum rising motion in the evening for the strong trade-wind days is ~35 cm s^{-1} (Fig. 21a), about 15–20 cm s^{-1} stronger than for the weak trade-wind days (Fig. 21b). Furthermore, the mixing ratio at low levels is 0.5 g kg^{-1} larger for the strong trade-wind days than for the weak trade-wind days (Figs. 21c,d). As a result, more rainfall occurs in this area when trades are stronger in agreement with YC03. The 4-h rainfall maximum (30–40 mm) for the strong trade-wind days shifts from the central Kona coast and lower slopes in the evening to the ocean near the coast around midnight (Figs. 20b,c).

Over northwest Hawaii, with descending downslope winds on the lee side with adiabatic warming and drying (Fig. 8), rainfall events are infrequent (Chen and Nash 1994). Rainfall in this area mainly occurs in afternoon hours under weak trade-wind conditions due to the convergence between the anabatic winds and descend-

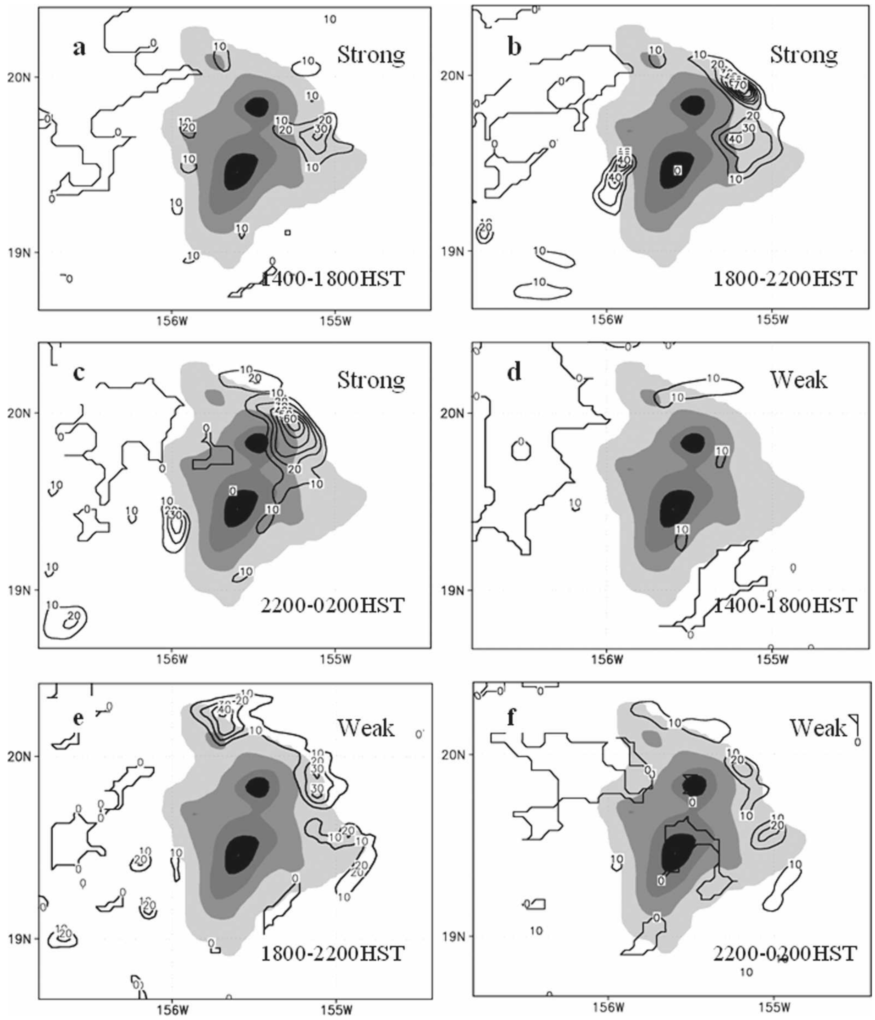

FIG. 20. The 4-h rainfall accumulation (mm) for the eight strong trade-wind days: (a) 1400–1800, (b) 1800–2200, and (c) 2200–0200 HST; and for the eight weak trade-wind days: (d) 1400–1800, (e) 1800–2200, and (f) 2200–0200 HST.

ing downslope winds (Schroeder 1981; YC03). When trades are stronger, with a stronger descending trade-wind flow from the upper slopes, the convergence between the anabatic winds and the descending flow yields a stronger vertical motion (Fig. 18e). However, under strong trades, the observed rainfall amount is less (YC03), with less simulated cloud water on the lee side (Fig. 16a) because of warmer (Fig. 12) and drier conditions in the lee as compared with weak trade conditions (Fig. 8).

4. Southeasterly trade-wind flow regime

Under a southeasterly trade-wind flow regime, there are differences in the location and strength of the lee vortices, depth of the reversed flow, thermodynamic fields, and rainfall production as compared with the easterly trade-wind flow regime. In this section, these differences will be presented.

a. Horizontal distribution of thermal fields

On the southwestern lee side of the island, the maximum temperature for the southeasterly trade-wind days (Fig. 22a) is about the same as for the strong trade-wind days, and 0.5 K higher than for the weak trade-wind days (Fig. 12). The descending flow aloft in the southwestern leeside area for the southeasterly flow is more significant, with stronger adiabatic warming than for a weak and normal trade-wind flow.

Similar to the trade-wind flow, the PV maxima occur on the northwestern and southwestern leeside areas of the island of Hawaii (Fig. 22b). On the northwestern lee side, the positive PV maximum under a southeast-

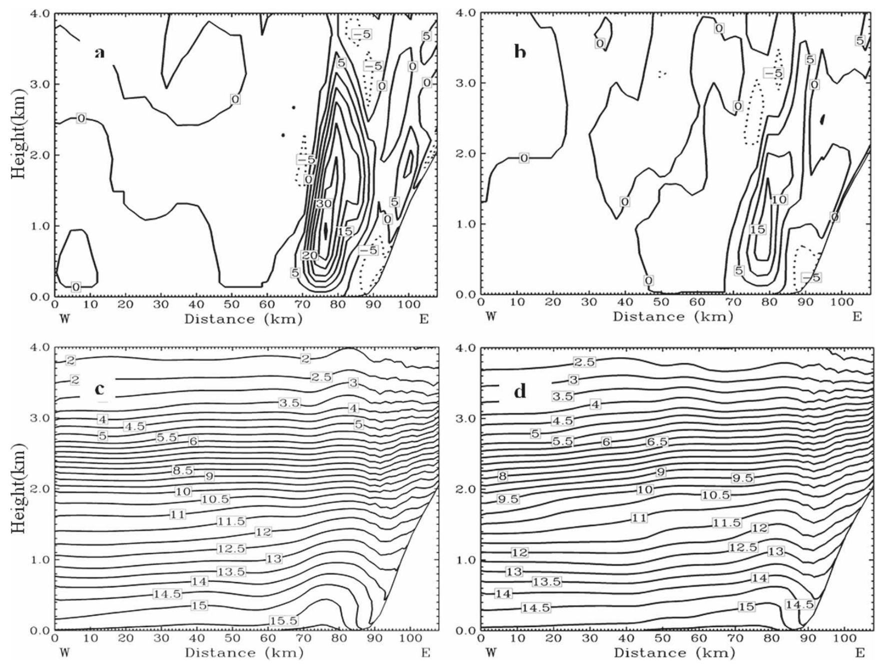

FIG. 21. Height–distance cross sections along the westerly revised flow of the large wake (the solid line in Fig. 4a). (a), (b) The mean vertical velocity at 2100 HST, CI = 5 cm s^{-1}, for (a) the eight strong, and (b) the eight weak trade-wind days and (c), (d) the mean mixing ratio, CI = 0.5 g kg^{-1}, for (c) the eight strong, and (d) the eight weak trade-wind days.

erly flow regime is 0.2–0.5 PVU smaller with a less pronounced cyclonic vortex than the trade-wind flow. On the southwestern lee side, for the five days with a southeasterly flow the negative PV maximum is 0.2 PVU larger, with a more pronounced anticyclonic vortex than for the trade-wind flow (Fig. 4).

b. Leeside circulations

Under a southeasterly flow regime, the wake zone (Fig. 23a) shifts northward as compared with the trade-wind flow (Fig. 4). The mean axis of the westerly reversed flow in the large wake is over the ocean off the northern Kona coast (19.6°N). Under the southeasterly flow regime, the southern anticyclonic lee vortex is more pronounced than under trade-wind conditions.

For the east–west cross section in the Kona area (Fig. 4a), the depth of the westerly reversed flow is 1.3 km (Fig. 23b), about 300 m lower than the trade-wind days. The trade-wind inversion heights determined from the Hilo soundings for the five southeasterly flow days are about 1.5 km, 300–400 m lower than that of the trade-wind flow. The trade-wind inversion acts as a lid to force the trade-wind flow to move around the island (Leopold 1949). With a lower trade-wind inversion, the wake circulation for the five southeasterly flow days is shallower than for the trade-wind days. The mean westerly reversed flow offshore under the southeasterly airflow is 0.5 m s^{-1} weaker (stronger) than for the strong (weak) trade-wind days (Fig. 5), most likely because of the difference in the strength of the incoming airflow between the trade-wind flow and the southeasterly flow (Table 1). Note the low-level southeasterly flows are 1 m s^{-1} weaker than the strong trade-wind flows and 2 m s^{-1} stronger than the weak trade-wind flows (Fig. 3).

With a wider mountain ridge facing the southeasterly flow than the east-northeasterly flow, the north–south extent of the wake zone with respect to the distance between the centers of the two lee vortices is larger for the southeasterly flow, consistent with idealized numerical studies (Smolarkiewicz and Rotunno 1989; and others).

In summary, under the southeasterly flow regime, the anticyclonic lee vortex is more pronounced than under the trade-wind flow with a larger negative PV maximum. The westerly reversed flow in the wake is shallower and shifts northward. The descending airflow aloft over the southwestern leeside slope for is more significant than for the trade-wind flow.

c. Rainfall

On the windward and leeside slopes of island of Hawaii, the maximum rainfall accumulation for the five

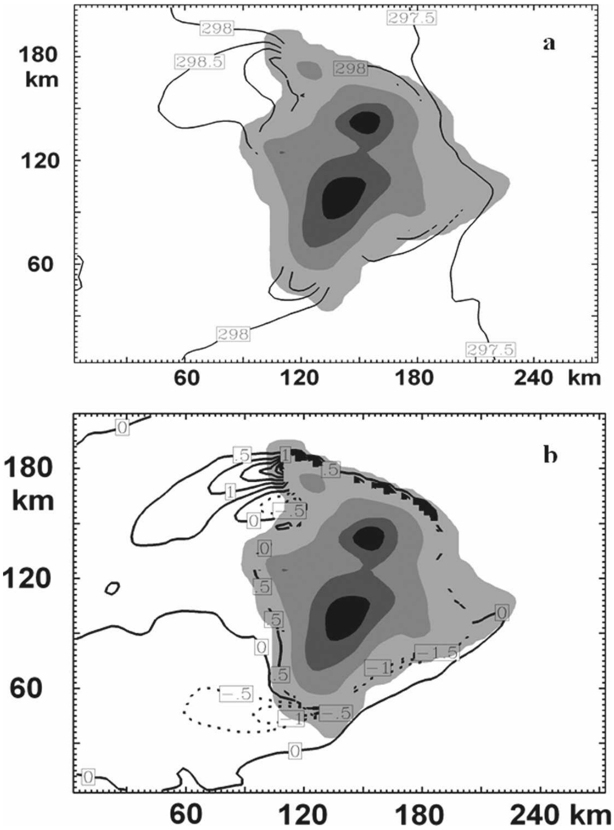

FIG. 22. (a) The mean potential temperature, CI = 0.5 K, and (b) the mean potential vorticity, CI = 0.5 PVU, at 500 m MSL for the five southeasterly trade-wind days.

days with a southeasterly airflow is around 10 mm (2 mm day^{-1}) (Fig. 23c). The maximum rainfall rate on the windward side of the island is much lower than that of the strong (18 mm day^{-1}) and the weak (8 mm day^{-1}) trade-wind days (Figs. 19a,b). As described above, the trade-wind inversion heights of the five days with a southeasterly flow are 300–400 m lower than that of the trade-wind flow. Lower trade-wind inversion height yields less rainfall on the windward side of the island of Hawaii (Chen and Feng 1995). Similar to the normal trade-wind cases, a maximum rainfall of 10 mm (2 mm day^{-1}) occurs over the ocean off the northern Kona coast in the evening and around midnight because of the convergence of the westerly reversed flow offshore and the katabatic/offshore flow at night (not shown). On the Kona slopes, rainfall occurs mainly in the afternoon hours because of the orographic lifting of the upslope flow.

5. Summary

The trade-wind flow upstream of the island of Hawaii has temporal variations in strength and direction, as a result, noticeable variations of the leeside circulations and weather are frequently observed. On the other hand, the land surface forcing during the diurnal cycle can affect the leeside circulations and weather. In this study, we investigate the effects of the trade-wind strength and directions, and modification of these effects by the land surface thermal forcing with MM5–LSM simulations classified for eight strong (7.9 m s^{-1}) and eight weak (5.2 m s^{-1}) trade-wind days and for five days with southeasterly trades (7.1 m s^{-1}) during summer 2004.

The large wake circulation off the Kona western leeside coast lies in the flow regime with counterrotating lee vortices, a westerly return flow along the wake axis, and splitting airflow on the windward side as the incoming trades encounter two massive volcanic mountains (Mauna Kea and Mauna Loa) with heights >4000 m, well above the typical height of trade-wind inversion (2000 m). The small wake on the lee side of the Kohala Mountains (1700 m) with mountaintops below the trade-wind inversion lies in the flow regime; thus, the trade-wind aloft can move over the mountains with westerly return flow in the wake with a hydraulic jump over the leeside slope. The response of wake circulations to variations in trade-wind strength and the diurnal heating cycle differs between the large wake and the small wake.

For the small wake, downslope winds are stronger with warmer and drier conditions on the leeside for the eight strong trade-wind days than for the eight weak trade-wind days. The westerly reversed flow in the small wake offshore is weaker (0.5 versus 2.5 m s^{-1}) for the eight strong trade-wind days as compared with the eight weak trade-wind days. In contrast, the westerly reversed flow along the large wake axis and the counterrotating vortices in the large wake are more significant with a stronger (1–1.5 m s^{-1}) and deeper (200–300 m) reversed flow with higher moisture content when trades are stronger. The deeper westerly reversed flow for the stronger trade-wind days may be related to the fact that the trade-wind inversion is higher for the strong trade-wind days than the weak trade-wind days (2100 versus 1850 m). The nondimensional westerly reversed wind speed (u/U) is about the same (0.4) for both cases.

Over the Kona slopes, less orographic cloudiness with more significant land surface heating occurs during the day under stronger trade-wind flow because of descending trade-wind flow aloft through the Humu'ula Saddle between Mauna Loa and Mauna Kea. Furthermore, for most of the weak trade days, the trade-wind inversion height (1850 m) is below the model terrain of the Humu'ula Saddle (>2000 m), preventing the trade-

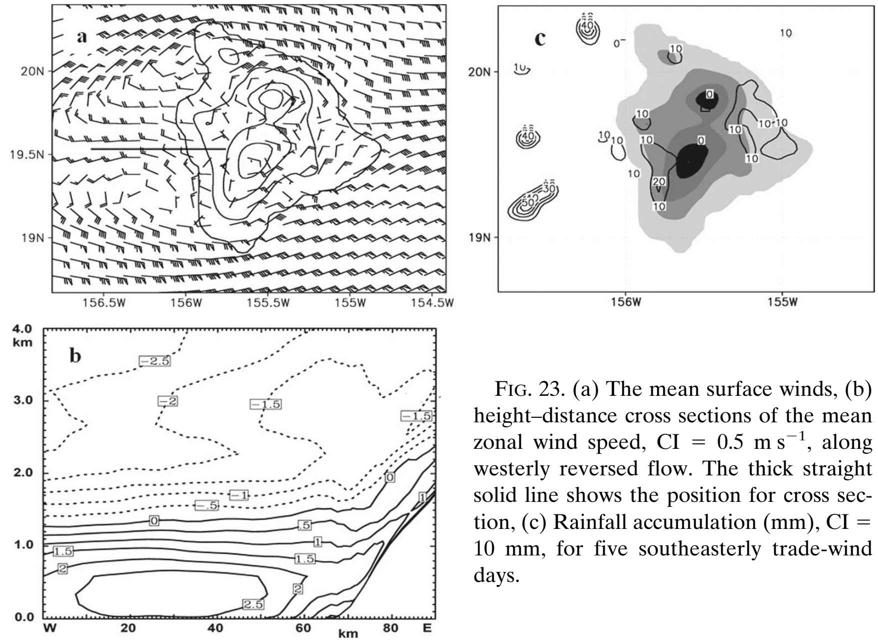

FIG. 23. (a) The mean surface winds, (b) height–distance cross sections of the mean zonal wind speed, CI = 0.5 m s^{-1}, along westerly reversed flow. The thick straight solid line shows the position for cross section, (c) Rainfall accumulation (mm), CI = 10 mm, for five southeasterly trade-wind days.

wind flow from penetrating the inversion and descending in the lee of the saddle. As a result, the daytime thermally direct circulation cell over the Kona coastal region and slope is more significant when trades are stronger. For the strong trade-wind days, the convergence between the westerly reversed flow offshore along the wake axis and the offshore/katabatic flow in the Kona coast region in the evening is more significant with stronger (35 versus 20 cm s^{-1}) rising motion and higher moisture content within the westerly reversed flow than for the weak trade-wind days. As a result, more evening rainfall occurs in this region when trades are stronger.

For both the strong and weak trade-wind days, the daytime flow regime over the Kohala Mountains over northern Hawaii is characterized by a reversed flow (4 m s^{-1}) off the leeside coast merging with sea breeze circulation over the coastal areas and lower leeside slopes. When trades are stronger, with a stronger descending trade-wind flow from the upper slopes, the convergence between the anabatic winds and the descending flow is greater, with a stronger vertical motion on the leeside slopes. However, there is less simulated cloud water under strong trades because of warmer and drier conditions due to a more significant adiabatic descent in the lee. At night, the flow regime for weak trade-wind days is characterized by a weak reversed flow (1 m s^{-1}) in the wake with descending airflow on the leeside slopes. The combined downslope/katabatic flow prevails on the lee side without a reversed flow offshore when trades are stronger.

Under the southeasterly trade-wind flow regime, the wake circulations of the large wake shift northward compared with the trade-wind flow. The distance between the two lee vortex centers under a southeasterly flow is wider than under a trade-wind flow. The westerly reversed flow in the wake is shallower, perhaps due to a lower (300 m) trade-wind inversion for a southeasterly flow than for a trade-wind flow. On the southwestern leeside area, the descending airflow aloft is more significant for a southeasterly flow with higher temperatures and a larger negative PV maximum than for an easterly trade-wind flow. For a southeasterly trade-wind flow, the anticyclonic vortex off the southwestern leeside coast is more pronounced than for a trade-wind flow.

Acknowledgments. We thank the NCAR MM5 group for the applications of the MM5–LSM, the anonymous reviewers for their comments, and D. Henderson for editing the text. We also thank Dr. W.-C. Lee of NCAR for his comments. This work is supported by the National Science Foundation under Grant ATM-0140387 and the U.S. Department of Agriculture under Cooperative Research Agreement 05-JV-11272165-015. We thank the University of Hawaii and the Maui High Performance Computing Center (MHPCC) for their support of this project.

REFERENCES

Buzzi, A., N. Tartaglione, and P. Malguzzi, 1998: Numerical simulations of the 1994 Piedmont flood: Role of orography and moist processes. *Mon. Wea. Rev.,* **126,** 2369–2383.

Carbone, R. E., J. D. Tuttle, W. A. Cooper, V. Grubišić, and W. C. Lee, 1998: Trade wind rainfall near the windward coast of Hawaii. *Mon. Wea. Rev.,* **126,** 2847–2863.

Chen, F., and J. Dudhia, 2001: Coupling an advanced land surface–hydrology model with the Penn State–NCAR MM5 modeling system. Part I: Model implementation and sensitivity. *Mon. Wea. Rev.,* **129,** 569–585.

Chen, S.-H., and Y.-L. Lin, 2005: Effects of moist Froude number and CAPE on a conditionally unstable flow over a mesoscale mountain ridge. *J. Atmos. Sci.,* **62,** 331–350.

Chen, Y.-L., and A. J. Nash, 1994: Diurnal variation of surface airflow and rainfall frequencies on the island of Hawaii. *Mon. Wea. Rev.,* **122,** 34–56.

——, and J.-J. Wang, 1994: Diurnal variation of surface thermodynamic fields on the island of Hawaii. *Mon. Wea. Rev.,* **122,** 2125–2138.

——, and J. Feng, 1995: The influences of inversion height on precipitation and airflow over the island of Hawaii. *Mon. Wea. Rev.,* **123,** 1660–1676.

——, and ——, 2001: Numerical simulations of airflow and cloud distributions over the windward side of the island of Hawaii. Part I: The effects of trade wind inversion. *Mon. Wea. Rev.,* **129,** 1117–1134.

Chu, C.-M., and Y.-L. Lin, 2000: Effects of orography on the generation and propagation of mesoscale convective systems in a two-dimensional conditionally unstable flow. *J. Atmos. Sci.,* **57,** 3817–3837.

Colle, B. A., 2004: Sensitivity of orographic precipitation to changing ambient conditions and terrain geometries: An idealized modeling perspective. *J. Atmos. Sci.,* **61,** 588–606.

Dudhia, J., 1993: A nonhydrostatic version of the Penn State–NCAR mesoscale model: Validation tests and simulation of an Atlantic cyclone and cold front. *Mon. Wea. Rev.,* **121,** 1493–1513.

——, and M. W. Moncrieff, 1989: A three-dimensional numerical study of an Oklahoma squall line containing right-flank supercells. *J. Atmos. Sci.,* **46,** 3363–3391.

Esteban, M. A., and Y.-L. Chen, 2008: The impact of trade wind strength on precipitation over the windward side of the island of Hawaii. *Mon. Wea. Rev.,* **136,** 913–928.

Feng, J., and Y.-L. Chen, 2001: Numerical simulations of airflow and cloud distributions over the windward side of the island of Hawaii. Part II: Nocturnal flow regime. *Mon. Wea. Rev.,* **129,** 1135–1147.

Fett, R. W., and S. D. Bury, 1981: Island barrier effects as observed by satellite and instrumented aircraft and simulated by a numerical model. *Mon. Wea. Rev.,* **109,** 1527–1541.

Grell, G. A., 1993: Prognostic evaluation of assumptions used by cumulus parameterizations. *Mon. Wea. Rev.,* **121,** 764–787.

Hong, S.-Y., and H.-L. Pan, 1996: Nonlocal boundary layer vertical diffusion in a medium-range forecast model. *Mon. Wea. Rev.,* **124,** 2322–2339.

Hsie, E.-Y., R. A. Anthes, and D. Keyser, 1984: Numerical simulation of frontogenesis in a moist atmosphere. *J. Atmos. Sci.,* **41,** 2581–2594.

Juang, H. H., 2000: The NCEP mesoscale spectral model: A revised version of the nonhydrostatic regional spectral model. *Mon. Wea. Rev.,* **128,** 2329–2362.

Leopold, L. B., 1949: The interaction of trade-wind and sea breeze, Hawaii. *J. Meteor.,* **6,** 312–320.

Li, J., and Y.-L. Chen, 1999: A case study of nocturnal rain showers over the windward coastal region of the island of Hawaii. *Mon. Wea. Rev.,* **127,** 2674–2692.

Miglietta, M. M., and A. Buzzi, 2001: A numerical study of moist stratified flow over isolated topography. *Tellus,* **53A,** 481–499.

Nickerson, E. C., 1979: On the numerical simulation of airflow and clouds over mountainous terrain. *Beitr. Phys. Atmos.,* **52,** 161–177.

——, and M. A. Dias, 1981: On the existence of atmospheric vortices downwind of Hawaii during the HAMEC project. *J. Appl. Meteor.,* **20,** 868–873.

Patzert, W. C., 1969: Eddies in Hawaiian waters. Hawaii Institute of Geophysics Rep. HIG-69-8, University of Hawaii, 51 pp.

Rasmussen, R. M., P. K. Smolarkiewicz, and J. Warner, 1989: On the dynamics of Hawaiian cloud bands: Comparison of model results with observations and island climatology. *J. Atmos. Sci.,* **46,** 1589–1608.

Reisner, J. M., and P. K. Smolarkiewicz, 1994: Thermally forced low Froude number flow past three-dimensional obstacles. *J. Atmos. Sci.,* **51,** 117–133.

Schär, C., and R. B. Smith, 1993: Shallow-water flow past isolated topography. Part I: Vorticity production and wake formation. *J. Atmos. Sci.,* **50,** 1373–1400.

Schroeder, T., 1981: Characteristics of local winds in northwest Hawaii. *J. Appl. Meteor.,* **20,** 874–881.

——, 1993: Climate controls. *Prevailing Trade Winds: Climate and Weather in Hawaii,* M. Sanderson, Ed., University of Hawaii Press, 12–36.

Smith, R. B., 1989: Hydrostatic flow over mountains. *Advances in Geophysics,* Vol. 31, Academic Press, 1–41.

——, and V. Grubišić, 1993: Aerial observation of Hawaii's wake. *J. Atmos. Sci.,* **50,** 3728–3750.

Smolarkiewicz, P. K., and R. Rotunno, 1989: Low Froude number flow past three-dimensional obstacles. Part I: Baroclinically generated lee vortices. *J. Atmos. Sci.,* **46,** 1154–1164.

——, R. M. Rasmussen, and T. L. Clark, 1988: On the dynamics of Hawaiian cloud bands: Island forcing. *J. Atmos. Sci.,* **45,** 1872–1905.

Ueyoshi, K., and Y.-J. Han, 1991: A three-dimensional simulation of airflow and orographic rain over the island of Hawaii. *J. Meteor. Soc. Japan,* **69,** 127–151.

Yang, Y., and Y.-L. Chen, 2003: Circulations and rainfall on the lee side of the island of Hawaii during HaRP. *Mon. Wea. Rev.,* **131,** 2525–2542.

——, and ——, 2008: Effect of terrain heights and sizes on island-scale circulations and rainfall for the island of Hawaii during HaRP. *Mon. Wea. Rev.,* **136,** 120–146.

——, ——, and F. M. Fujioka, 2005: Numerical simulations of the island-induced circulations over the island of Hawaii during HaRP. *Mon. Wea. Rev.,* **133,** 3693–3713.

Zhang, Y., Y.-L. Chen, S.-Y. Hong, H. H. Juang, and K. Kodama, 2005a: Validation of the coupled NCEP mesoscale spectral model and an advanced land surface model over the Hawaiian Islands. Part I: Summer trade wind conditions and a heavy rainfall event. *Wea. Forecasting,* **20,** 847–872.

——, ——, T. A. Schroeder, and K. Kodama, 2005b: Numerical simulations of the sea-breeze circulations over northwest Hawaii. *Wea. Forecasting,* **20,** 827–846.